DEPENDENCE OF STELLAR SUBSTRUCTURES IN M31 TYPE GALAXY ON SATELLITE MORPHOLOGY IN GALAXY MERGERS

S. Milošević

University of Belgrade, Department of Astronomy at Faculty of Mathematics,
Studentski trg 16, 11000 Belgrade, Serbia

E–mail: *stanislav@matf.bg.ac.rs*

SUMMARY: Stellar streams and shells are observed in halos of spiral galaxies. In this paper, we investigated the formation of these structures due to mergers between the host spiral galaxy and its dwarf satellite galaxies. We run the N-body simulations with two morphological models of a dwarf galaxy for different initial positions. One model is a spheroidal dwarf, dSph, and the other is a dwarf with a disk. We found that both models form stellar shells and streams and, in the case of the progenitor with a disk, streams are more prominent. After several pericentric passages, there is a possibility of formation of several streams. The remnant of the progenitor is more likely to disrupt later into the merger in the case of spiral progenitor than in the case of dSph.

Key words. Galaxies: interactions – Galaxies: dwarf – Methods: numerical

1. INTRODUCTION

Tidal structures such as tidal tails, shells, and stellar streams, are discovered in many spiral and elliptical galaxies. These structures are formed in merger events. Galaxy mergers are very important in the standard hierarchical cosmological picture. Large mass galaxies are growing by mergers of the smaller ones (Purcell et al. 2007). The existence of these tidal structures and knowledge of their properties such as spatial extent, velocity distribution, and metallicities, give an opportunity to understand the merger history and properties of galaxies included in a particular merger. Properties of the substructures depend on many parameters like mass ratios, initial distance, initial velocity, orbit inclination of the satellite galaxy, and morphology of the galaxies incorporated in a merger event.

Stellar streams and shells are observed in haloes of massive galaxies (Atkinson et al. 2013, Hood et al.

2018). In the Local Group, the Magellanic Stream is discovered between the Magellanic Clouds (Wannier and Wrixon 1972, Mathewson et al. 1974) and the Giant Stellar Stream (GSS) is discovered in the M31 galaxy (Ibata et al. 2001) as well as the NE and W shelf (Ferguson et al. 2002). The overview of the properties of the Magellanic Stream is given in Putman et al. (2002) and D'Onghia and Fox (2016). The work of Martínez-Delgado et al. (2010) gives several stellar structures formed in processes of galaxy mergers. Structures in the halo of M31 are formed by accretion of the satellite galaxy or galaxies. Many observations are done in the last two decades and properties of the structures are determined. The orientation and spatial extent of the GSS are given in works of McConnachie et al. (2003), and Conn et al. (2016), velocities properties in Ibata et al. (2004), Guhathakurta et al. (2006), Gilbert et al. (2009), and metallicities in Ibata et al. (2007), Gilbert et al. (2009, 2018), Conn et al. (2016), Cohen et al. (2018), Escala et al. (2021). Data from observations (e.g. Merritt et al. (2016)) unlocked the possibility and gave parameters for theoretical probing of models of galaxies in merger events.

Many theoretical works were done to explain the existence of tidal structures in different merger scenarios and the possibility of their observation due to low surface brightness (Johnston et al. 2008). Disruption of satellite galaxies is a common scenario for formation of those structures (Zolotov et al. 2009, Cooper et al. 2013, 2015, Longobardi et al. 2018, Karademir et al. 2019). The works of Pillepich et al. (2014) and Remus et al. (2017), discuss the connection between the shape of the outer halo and the merger history. In Karademir et al. (2019) different N-body simulations were done to find the properties of tidal structures. There are models for spiral galaxies, where the satellite galaxies are downscaled spirals of the host galaxy (Karademir et al. 2019). Properties of the structures were discussed for different merger scenarios, in particular for different mass ratios and different position angles, which leads to different orientations of angular momentum. It is given in Amorisco (2015) that these mergers are highly radial and that the satellite galaxy passes near the center of the host galaxy. Different mass ratios give different types of merger: the major, mini, and minor. In Karademir et al. (2019) it is shown that the minor and mini mergers are important for formation of tidal features.

Some observed properties of the GSS and shells in the halo of the M31 were reproduced with both models - a satellite with and without a disk. The morphology of satellite galaxy was discussed in Fardal et al. (2006, 2007) and Sadoun et al. (2014) where the formation of the GSS was analyzed. Fardal et al. (2007) and Sadoun et al. (2014) used a satellite galaxy with a disk and a spherical galaxy without a disk, while Miki et al. (2016) used a disky satellite. In Milošević et al. (2022), the dSph galaxy was used as the GSS progenitor to explain the metallicity distribution along the GSS.

In this paper, we investigate the influence of morphology of the satellite galaxy on formation of tidal structures in the host galaxy in merger events. Two morphological types of satellite galaxy were used: the spherical galaxy and galaxy with a disk. In both scenarios, a similar mass ratio was used and the same initial distance for different position angles.

This paper is organized as follows: Section 2 gives N-body models for the host galaxy and satellites with different morphology, in Section 3 we present the main results of merger events, and the discussion and conclusion are given in Section 4.

2. METHODS

2.1. N-body models

We used an N-body representation for the host spiral galaxy and satellite galaxies. The main morphological parts of the host galaxy are a spherical bulge, exponential disk, and dark matter halo. This model corresponds to the M31-like galaxy. A sim-

ilar model is used in Geehan et al. (2006), Fardal et al. (2007), Sadoun et al. (2014) and Milošević et al. (2022). Pure N-body models for all three types of galaxies are generated with the GalactICs package (Widrow et al. 2008).

Density profiles of all three components in the host galaxy and dSph are taken from Milošević et al. (2022) and these profiles are similar to one given in Geehan et al. (2006) and Sadoun et al. (2014). These density profiles are well established and used in previous N-body models for spiral galaxies similar to the Milky Way and M31 galaxies, and also for dwarf galaxies with or without a disk. The bulge is represented with the Prugniel-Simien profile (Widrow et al. 2008):

$$\rho_{\rm b} = \rho_{\rm b0}\left(\frac{r}{r_{\rm b}}\right)\exp\left(r/r_{\rm b}\right)^{-1/n}. \qquad (1)$$

Here, $\rho_{\rm b0}$ is the density at $r = r_{\rm b}$, and $r_{\rm b}$ is the bulge scale radius.

The disk is represented by a combination of two profiles: an exponential profile of surface density in the $x - y$ plane and the sech^2 law in the vertical, z-direction. The exponential profile is given by (Geehan et al. 2006, Sadoun et al. 2014):

$$\Sigma(R) = \frac{M_{\rm d}}{2\pi R_{\rm d}^2}e^{-\frac{R}{R_{\rm d}}}. \qquad (2)$$

Here, $M_{\rm d}$ is the total mass of the disk, Σ is the surface density and $R_{\rm d}$ is the disk scale radius. In the last two equations, r is the spherical radius and R is the cylindrical radius.

The sech^2 profile is used in vertical z-direction (Sadoun et al. 2014) and the combined profile is given by:

$$\rho(R, z) = \frac{\Sigma(R)}{2z_0}{\rm sech}^2\left(\frac{z}{z_0}\right). \qquad (3)$$

Here, z_0 is the scale height of the disk. The inclination of the disk is 77 degrees, the position angle is 37 degrees (Fardal et al. 2007), and the heliocentric distance to Andromeda is taken to be 785 kpc.

A spherical dark matter halo is a more general form of the Navarro-Frenk-White profile (Navarro et al. 1996) given in GalactICs (Widrow et al. 2008):

$$\rho(r) = \frac{2^{2-\alpha}\sigma_{\rm h}^2}{4\pi r_{\rm s}^2}\frac{\rho_0}{(r/r_{\rm s})^\alpha(1 + r/r_{\rm s})^{3-\alpha}}\frac{1}{2}{\rm erfc}\left(\frac{r - r_{\rm h}}{\sqrt{2}\delta_{r_{\rm h}}}\right). \qquad (4)$$

Here, all parameters are the same as in Milošević et al. (2022): $r_{\rm h}$ is the halo radius at which the density starts decreasing, $\sigma_{\rm h}$ is the typical velocity, $\delta_{r_{\rm h}}$ is the distance along which the density falls to zero, $r_{\rm s}$ is the scale radius for halo, and α is an exponent in the NFW profile and we took $\alpha = 1$. The total mass of the host galaxy is the same as for M31 in Milošević
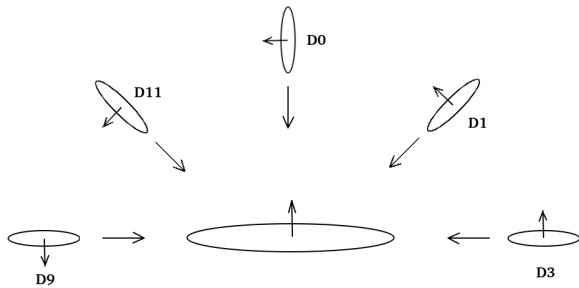
Fig. 1: The initial positions for dwarf progenitor with a disk, D models. The positions for the S3, S1, and S0 models were used in simulations with the dSph model of progenitor. The last two positions are symmetric with the first two for the dSph model.

et al. (2022) as well as the values for the host galaxy parameters.

For the satellite galaxies we used two models: the first one is the dSph model and the second is a dwarf with a disk. Both models contain a spherical bulge of baryonic matter and a spherical dark matter halo. The second model contains a baryonic disk unlike dSph, represented with the same density profile as that for the disk of the host. The parameters used for generating models of these two galaxies are given in Table 1.

2.2. Merger Parameters

We set up eight initial positions for merger events for five position angles between the disk of the host and the directions to the infalling satellite. In Karademir et al. (2019) five orbits were tested to describe how the structures are forming due to different infall. Here, we are interested in how morphology affects the formation of tidal structures due to different infall. Three positions were tested for the dSph model, and two additional for the dwarf with a disk. These additional two positions for the dwarf with a disk were tested because of different directions of the angular momentum. The position angles are 0, 45, 90, 135, and 180 degrees as seen in Fig. 1. All galaxies start their infall from the distance of 100 kpc due to timescale of the tidal strucsture formation described in previous works (Sadoun et al. 2014, Hammer et al. 2018, Milošević et al. 2022). We named these models D3, D1, D0, D11, and D9, respectively, in the case of the dwarf with a disk, and S3, S1, and S0 for the dSph progenitor. The model labeling numbers are taken in the counterclockwise direction. To run simulations we used the cosmological simulation code Gadget2 (Springel 2005).

3. RESULTS

We present the merger history and formation of structures for different initial positions of the satellite galaxy. The comparison is made between two different morphologies and different orientations of mo-

mentum vectors of the host and satellite galaxy. In Fig. 2 and Fig. 3 we can see the merger history of the dSph galaxy for three different initial positions due to the characteristic trajectory of infall. We traced the progenitor galaxy from the beginning of the simulation till 2 Gyrs. The initial position is 100 kpc with null initial velocity and the first pericentric passage occuring after 0.6 Gyrs. In three simulations the inclination angles were 0, 45, and 90 degrees with respect to the disk of the host galaxy.

For the progenitor with a disk, we presented five simulations with characteristic orientations of the momentum vectors. As in the previous case, the initial position is 100 kpc with null velocity. Fig. 4 presents merger events for initial angles: 0, 45, 90, 135, and 180 degrees, in other words, the models D3, D1, D0, D11, and D9. Again, we traced the merger history to 2 Gyrs after several pericentric passages. The timescale of the merger events and several orbits of the progenitor galaxy are presented in Figs. 2, 3, and 4. After 2 Gyrs, the progenitor galaxy makes several orbits around the host galaxy and experiences a tidal disruption.

In the mass density plot presented in Fig. 5 we can see more clearly the formation of morphological substructures such as shells and streams. Also, it is possible to trace the remnant of the progenitor. In this figure, we present the merger event between 1 and 2 Gyrs, after the second and third pericentric passage.

In Fig. 6 we can see the mass density plots for the case of D models. In the case of models D1 and D11, more clear substructures are formed. In all simulations after 1 Gyr, there are strong stellar streams and shells. After several pericentric passages, streams become faint, and shells are more prominent. We can also trace the progenitor remnant in all cases till it finally disrupts.

Morphological substructures that are produced by merger events are represented in phase-space plots. These are $d - v$ plots, where d is the radial distance of the particles from the center of the host galaxy, and v is the velocity. In Fig. 7, phase-space plots for the three different initial positions of the dSph and the progenitor with a disk are represented. In the first row in Fig. 7, the merger for the case of 0 degrees, the D3 model, we can see the formation of one stream after the second pericentric passage and two shells. After 1.4 Gyrs there are two stellar streams and two shells. We can also see the remnant of the satellite galaxy in one of the shells. We have a similar situation in the case of the D9 model, in the second row. There are also two streams and two shells after 1.4 Gyrs and a visible remnant of the progenitor galaxy. In panels: i, j, k, and l the infall of the dSph galaxy, the S3 model, is represented.

We can see the formed shells and one prominent stellar stream after the second passage, but later, the stream became faint and the remnant of the progenitor is disrupted.

Table 1: The values of parameters for the N-body model of progenitor galaxy. Similar values for the baryonic matter are used in Sadoun et al. (2014).

dSph					
Baryonic matter			$r_\mathrm{b} = 1.03$ kpc	$\sigma_\mathrm{b} = 93$ km/s	$M_\mathrm{s} = 2.18 \times 10^9 M_\odot$
Dark matter halo			$r_\mathrm{h} = 5$ kpc	$\sigma_\mathrm{h} = 185$ km/s	$M_\mathrm{h} = 2.4 \times 10^{10} M_\odot$
Dwarf disk					
Baryonic matter	$M_\mathrm{d} = 1.69 \times 10^9 M_\odot$	$r_\mathrm{d} = 0.8$ kpc			$M_\mathrm{s} = 2.18 \times 10^9 M_\odot$
	$M_\mathrm{b} = 0.49 \times 10^9 M_\odot$	$r_\mathrm{b} = 0.4$ kpc	$\sigma_\mathrm{b} = 78$ km/s		
Dark matter halo			$r_\mathrm{h} = 5$ kpc	$\sigma_\mathrm{h} = 127$ km/s	$M_\mathrm{h} = 2.2 \times 10^{10} M_\odot$
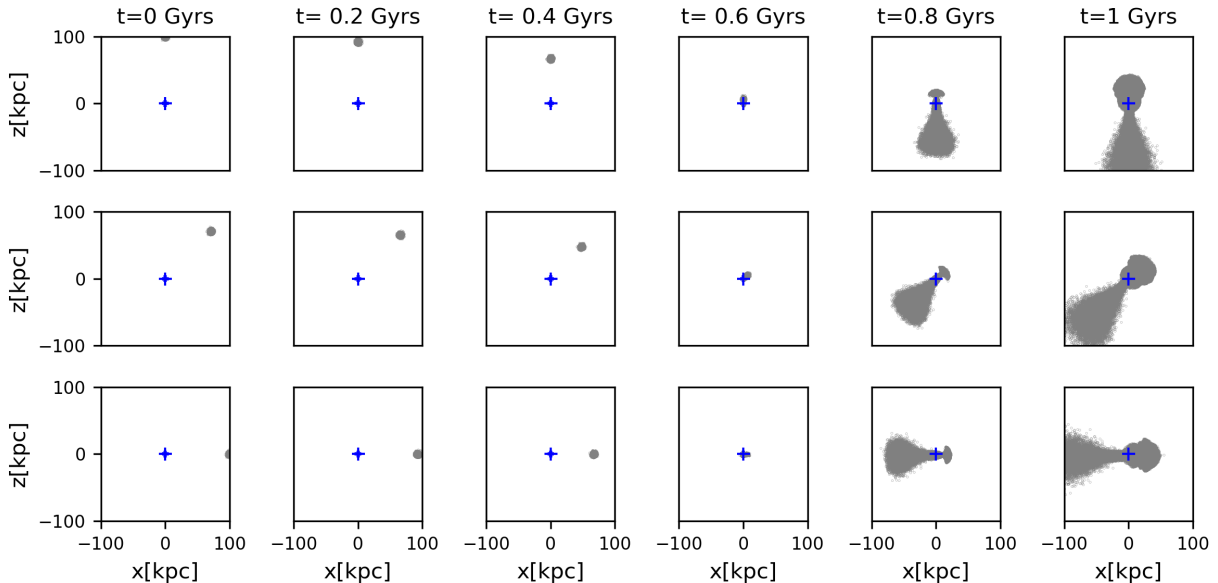
Fig. 2: Merger history for the dSph progenitor from the beginning of simulation till 1 Gyrs. Gray dots represent a satellite galaxy and the center of the host is represented by a blue dot. Particles of the host are omitted for better visibility. The upper row represents the merger for the S0 progenitor model, the middle row for S1, and the bottom row for S3.

Morphology is more important for the substructure formation than the direction of rotation of the same model, as we expected, but the influence of the momentum vector of the disk progenitor is not negligible.

In Fig. 8 we can see a phase-space plot for spiral progenitors with the D1 and D11 models, and the dSph progenitor, the S1 model. In all three cases, we see formed streams and shells. In the case of the S1 model, we see two streams after 1.4 Gyrs, and in the case of the S1, presented in panels: i, j, k, and l, only one stream. There is a clear influence of morphology on substructure formation. These models represent infall when the orbit of the progenitor is not in the same plane as the disk of the host, and also it is not along the z-axes as it was the case with the S0 and D0 models.

A similar situation we have in the case of the angle of 90 degrees in both progenitors, with a disk and the dSph. On highly radial orbits they form sub-

structures in the halo of the host galaxy. In Fig. 9, the upper row is the D0 model, and the bottom row is the S0 model. For the dSph progenitor, after 1 Gyr it is hard to follow the remnant of the progenitor and the formed stream becomes faint due to dynamical evolution. The infall angle affects the formation of shells and streams and in the case of models D1, D11 and S1 the formed structures are more prominent and live longer than in the cases D0 and S0.

The influence of rotation is presented in Fig. 10. The upper row shows the formed shells and the stream in the D3 scenario, where the momentum vectors of progenitor and host galaxy are parallel. In the bottom row, we represent the D9 scenario, where the momentum vectors are antiparallel. Both cases are represented for $t = 1$Gyrs, after several orbits of a satellite galaxy. We can see that the direction of rotation influences structure forming after the merger. In the case of the same directions of the host and satellite, in the D3 scenario, we have one stream and
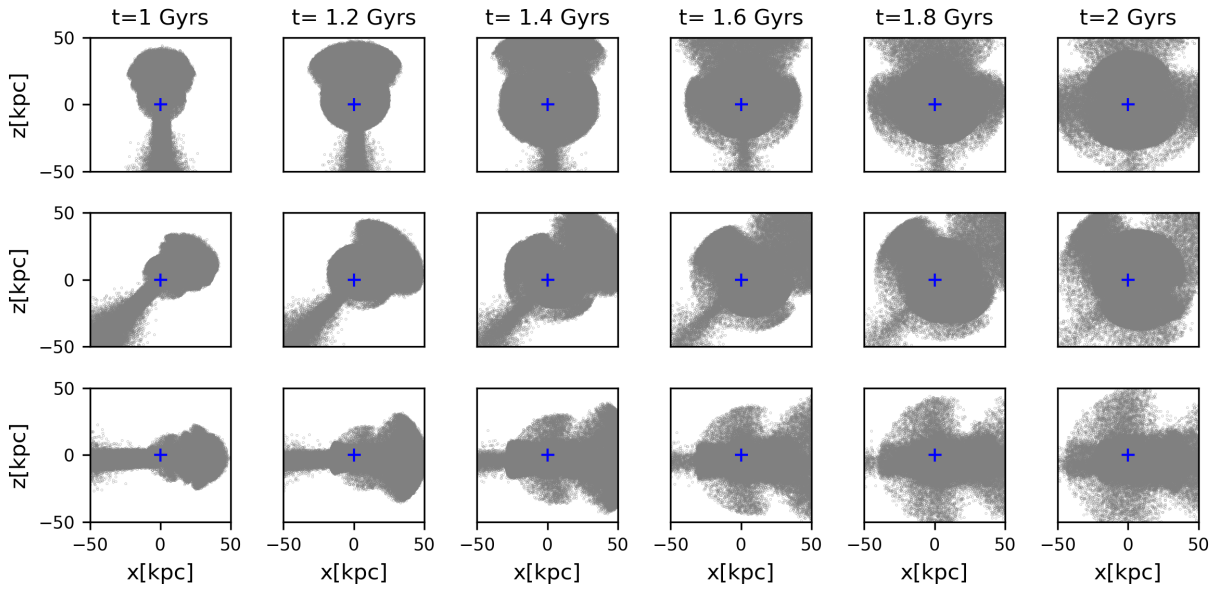
Fig. 3: Merger history for the dSph progenitor between 1 and 2 Gyrs. Symbols and rows represent the same as in Fig. 2.
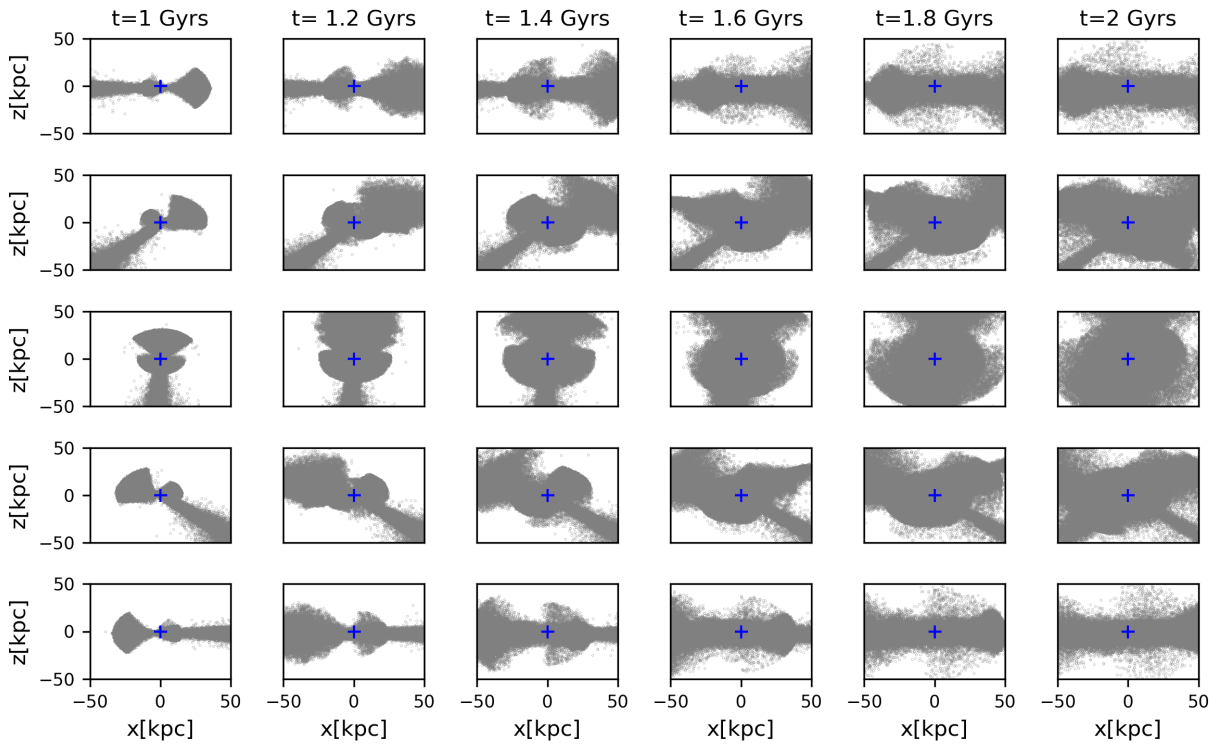
Fig. 4: Merger history for the progenitor with a disk, between 1 and 2 Gyrs. Gray dots represent a satellite galaxy and the center of the host is represented by a blue dot. Particles of the host are omitted for better visibility. Rows from top to bottom correspond to models D3, D1, D0, D11, and D9, respectively.
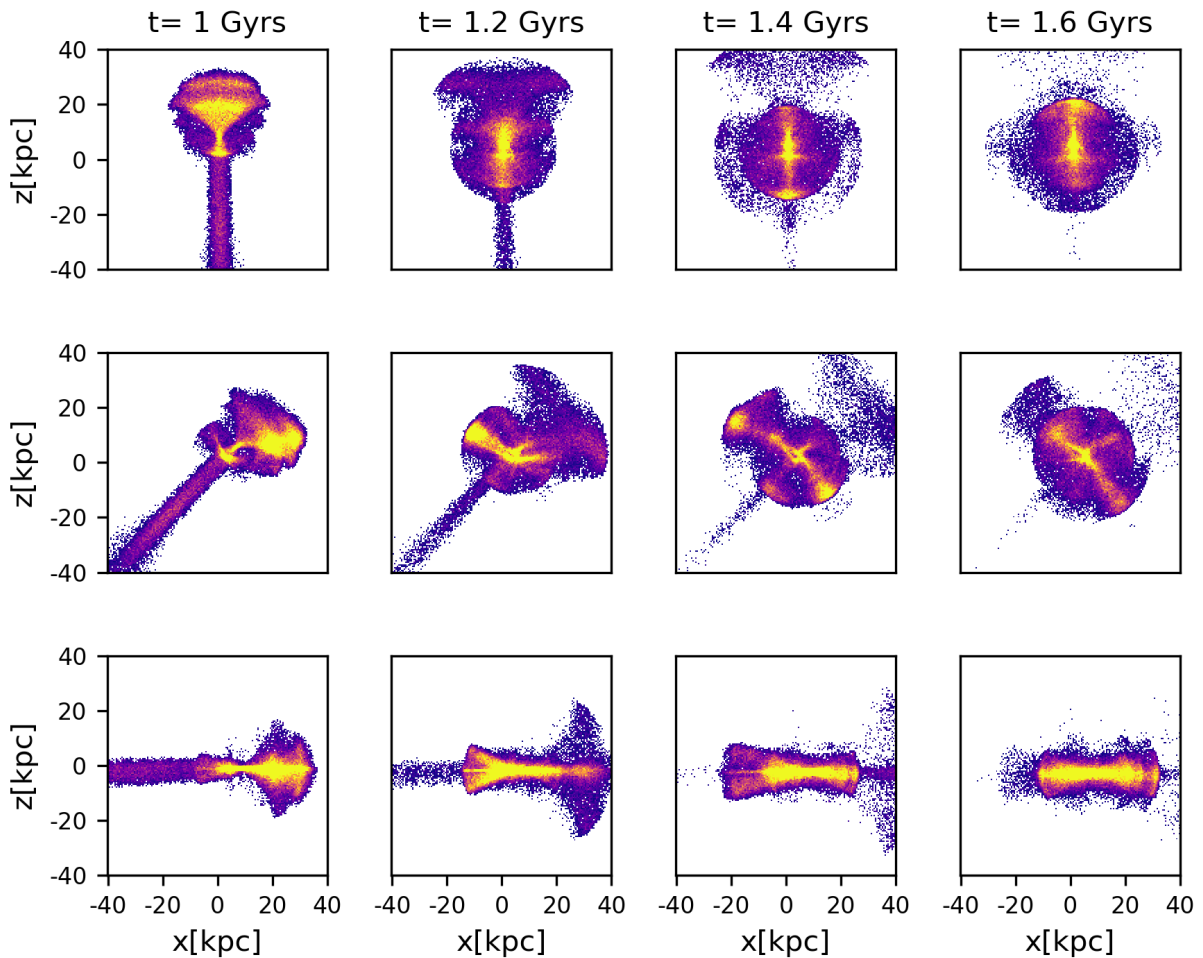
Fig. 5: The surface density plots for the S0, S1, and S3 models, from top to bottom, for the interval between 1 and 1.6 Gyrs.

two shells, and a similar situation in the D9 case. It is possible to follow the remnant of the progenitor later into the merger in the D3 case, than in D9. The scenario of forming structures is similar in these two merger events but there are differences in the way how the progenitor galaxy is disrupted because, in the case of disks with parallel momentum vectors, the remnant of the progenitor disrupts later.

We directly compare satellites with different morphology in Fig. 11. In the upper row, the model D1 is presented while the model S1 is shown in the bottom row. In the case of the progenitor with a disk, we can see two shells and one stream and all structures are more prominent than in the case S1. Both galaxies have the same initial position and velocities as well as the initial orbit inclination of 45 degrees. In the case of the galaxy with a disk, we have a more visible remnant, while in the case of dSph, after 1 Gyrs, the remnant started to disrupt, and it is in one of the shells. We can see that morphology plays the main role in shell formation, and shells are more prominent

in D models and so is also the remnant of the progenitor galaxy. Besides the progenitor morphology, the direction of rotation and infall angle also affect the formation of streams and shelves in merger events.

4. DISCUSSION AND CONCLUSIONS

In this paper, we investigated how different morphologies of the progenitors influence forming structures in the mergers between the host galaxy and satellites. We ran pure N-body simulations with two models of progenitor galaxies: dSph and progenitor with a disk. In the case of structures formed after the merger in the halo of the host, it is sometimes unclear which morphology type of the progenitor produced those structures. Mass, initial position and velocity are the main parameters that dictate the merger events. We showed that in both cases of the morphology of the progenitor, stellar streams and shells are formed.
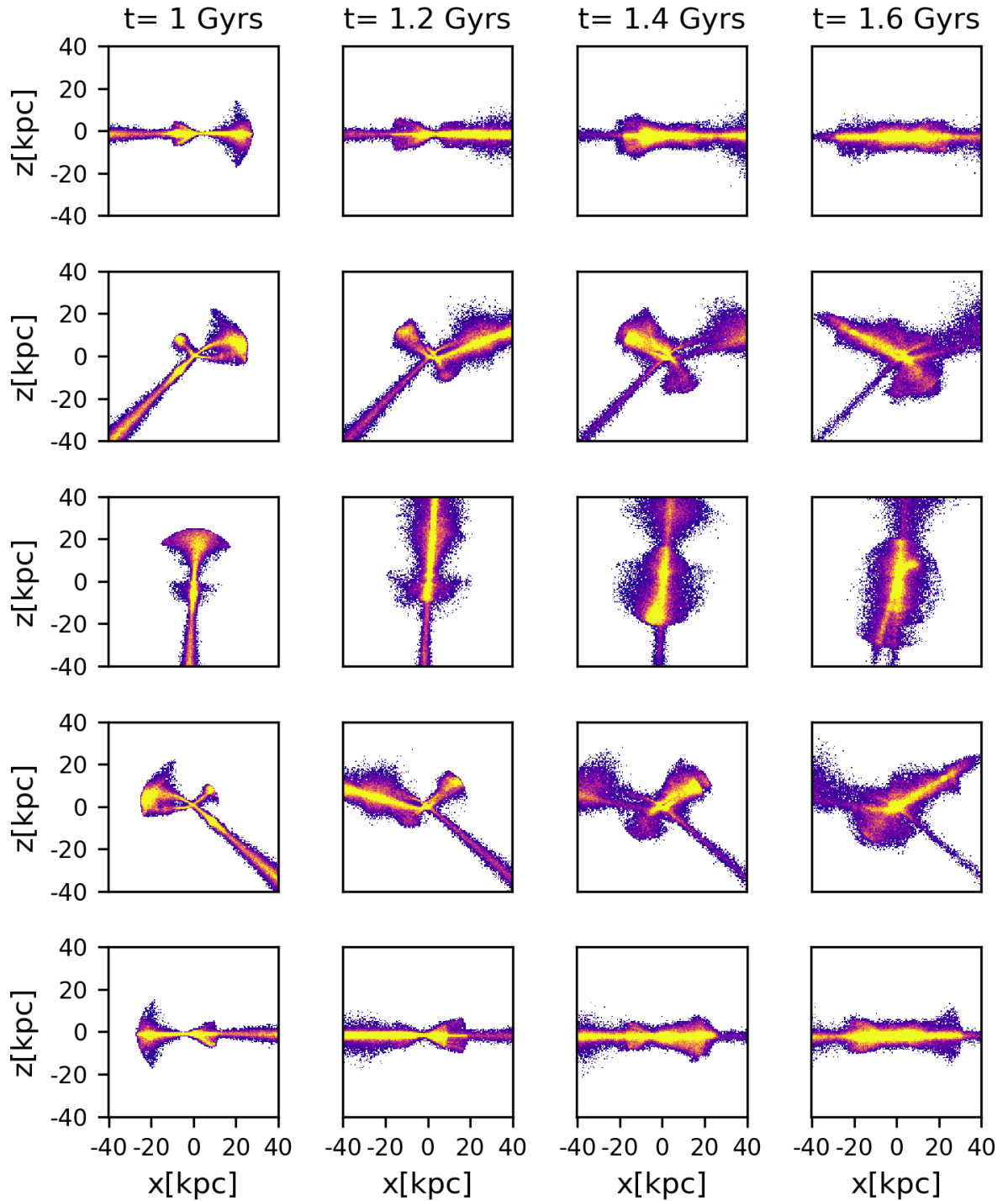
Fig. 6: The surface density plots for the D3, D1, D0, D11, and D9 models, from top to bottom, for the interval between 1 and 1.6 Gyrs.

We showed that beside mass, different morphologies produce different shells and streams. In some cases, streams are more prominent. In the case of the progenitor with a disk, and after several pericentric passages, there is more than one stream. Also, in the case of the satellite galaxy with a disk, it is possible to follow the remnant of the galaxy later into the merger.
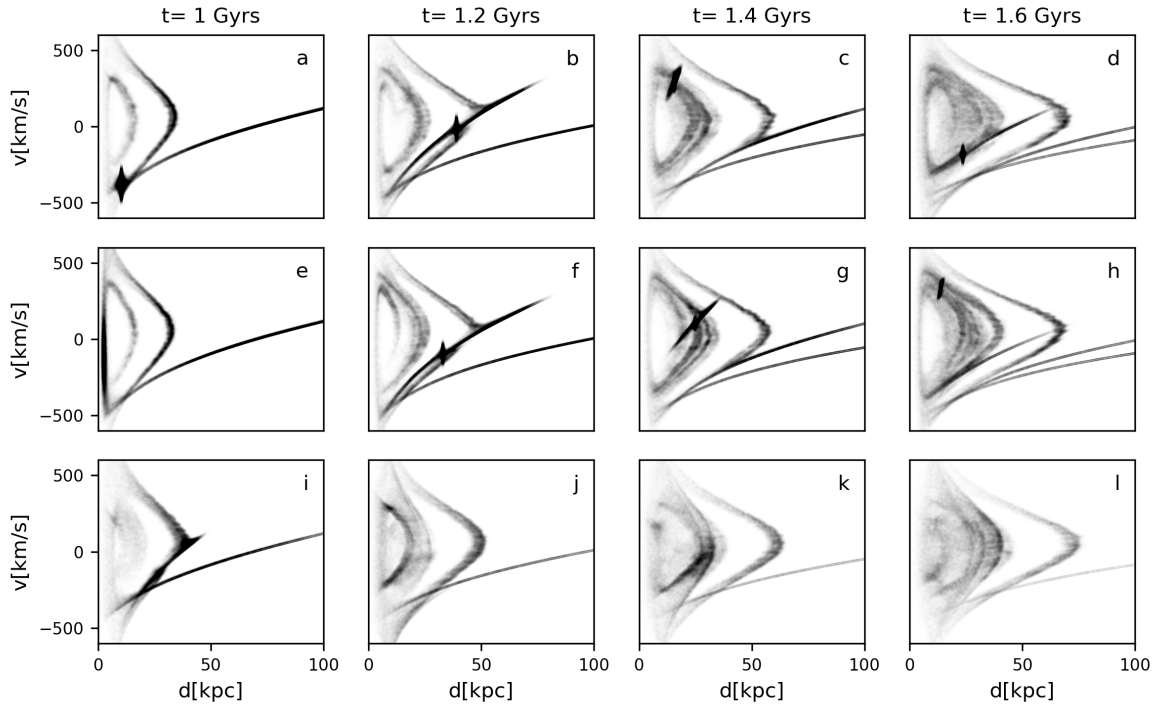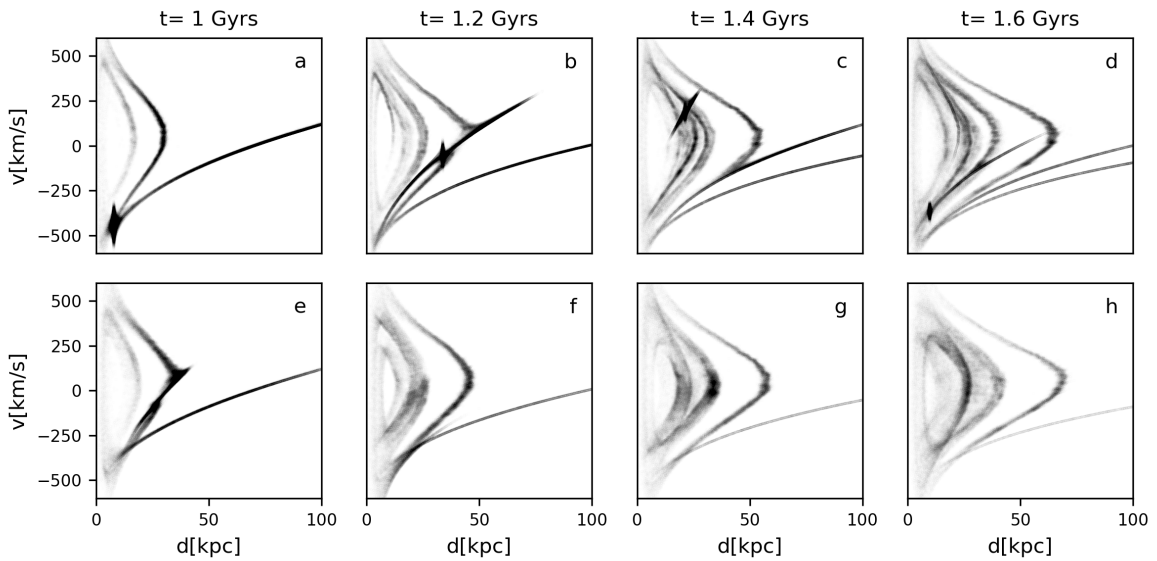
Fig. 7: The phase-space plots for timescales ranging from 1 to 1.6 Gyrs. The upper row is the D3 model, the middle row shows the D9 model, and the bottom row is for the S3 model.
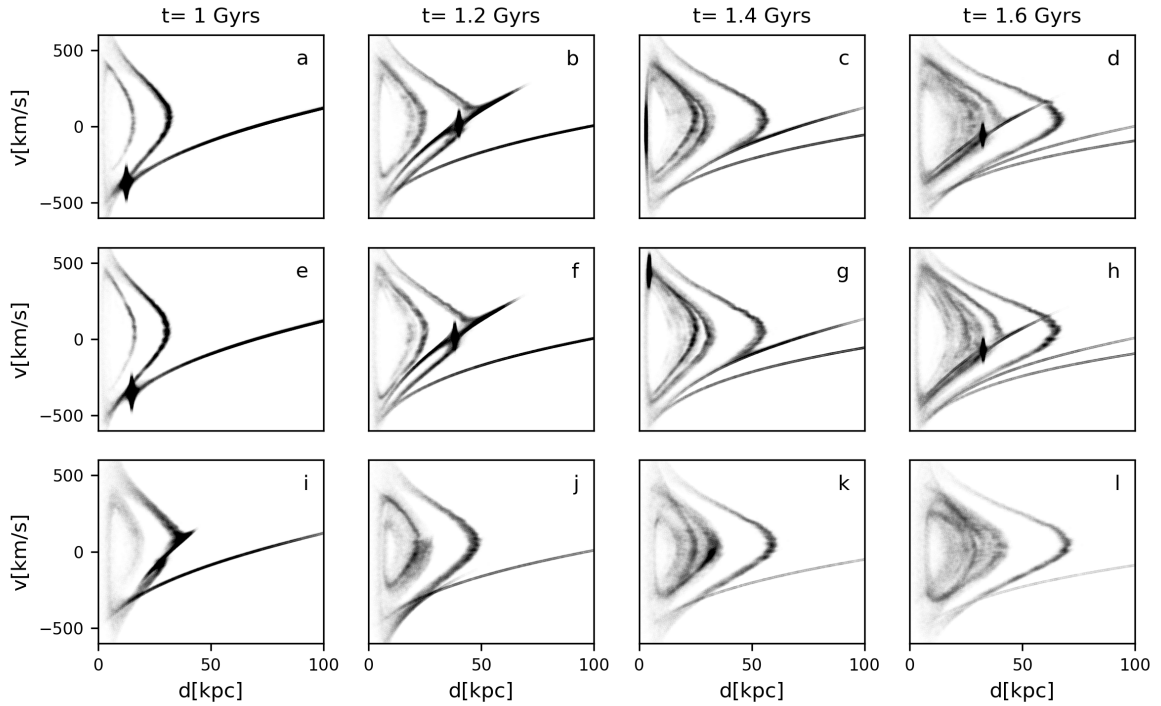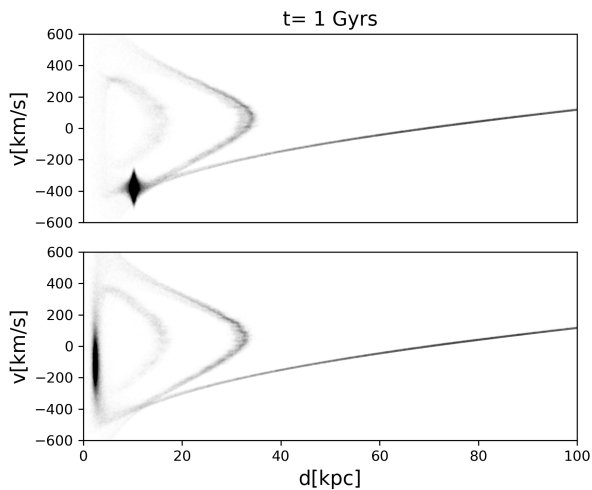

Fig. 8: The phase-space plots for timescales ranging from 1 to 1.6 Gyrs. The upper row is the D1 model, the middle row is the D11 model, and the bottom row is the S1 model.
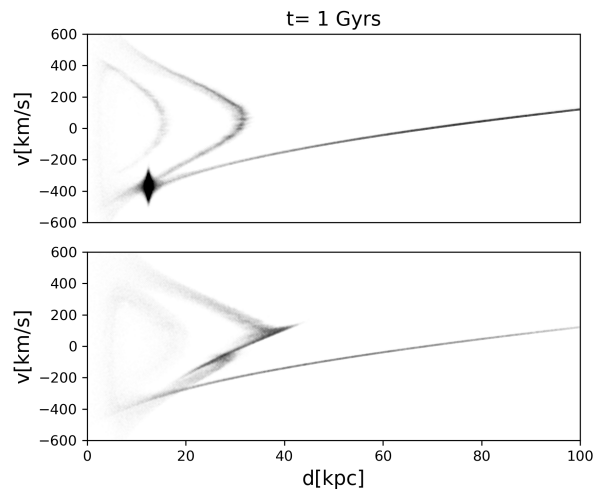
40

Fig. 9: The phase-space plots for timescales ranging from 1 to 1.6 Gyrs. The upper row is the D0 model, and the bottom row is the S0 model.

Fig. 10: The phase-space plots at 1Gyrs. The upper row is the D3 model, and the bottom row is the D9 model.

Fig. 11: The phase-space plots at 1Gyrs. The upper row is the D1 model, and the bottom row is the S1 model.

The dSph galaxy also forms structures, similar to D models. Stellar streams are faint and there is only one stream even after several orbits. There are also formed shells. Two observed streams in halos of the host can indicate the progenitor with a disk, but for a single stream we need additional constraints. In both models, S, and D, the orbit inclination plays a role, because we have a different shape of the formed structures; a similar result is given in Karademir et al. (2019).

In this paper, we also investigated the orientation of the satellite galaxy. The orientation of the progenitor with a disk is not negligible in a merger, because

there isn't the same scenario when we have parallel and antiparallel momentum vectors of the host and progenitor. The direction of the rotation of the progenitor with a disk is a parameter that influences the distribution of particles in a merger event. Although we have two shells and one stream in the D3, as well as in the D9 model, we can trace the remnant of the progenitor in the case of parallel momentum vectors in the D3 model.

In our simulations, the largest influence on the substructure formation has the morphology of the progenitor. The orientation of orbit, and also the orientation of the rotation for the disk progenitor, plays

an important role, especially in shelf formation and the timescale of the remnant disruption. The shelves are more prominent in the case of orbit with inclination of 45 degrees than in the cases of 0 and 90 degrees.

The observed properties of structures in halos of massive galaxies, such as streams and shells, can give constraints not only on the merger history, and timescale, but also on the morphology of the progenitor.

REFERENCES

Amorisco, N. C. 2015, MNRAS, 450, 575

Atkinson, A. M., Abraham, R. G. and Ferguson, A. M. N. 2013, ApJ, 765, 28

Cohen, R. E., Kalirai, J. S., Gilbert, K. M., et al. 2018, AJ, 156, 230

Conn, A. R., McMonigal, B., Bate, N. F., et al. 2016, MNRAS, 458, 3282

Cooper, A. P., D'Souza, R., Kauffmann, G., et al. 2013, MNRAS, 434, 3348

Cooper, A. P., Parry, O. H., Lowing, B., Cole, S. and Frenk, C. 2015, MNRAS, 454, 3185

D'Onghia, E. and Fox, A. J. 2016, ARA&A, 54, 363

Escala, I., Gilbert, K. M., Wojno, J., Kirby, E. N. and Guhathakurta, P. 2021, AJ, 162, 45

Fardal, M. A., Babul, A., Geehan, J. J. and Guhathakurta, P. 2006, MNRAS, 366, 1012

Fardal, M. A., Guhathakurta, P., Babul, A. and McConnachie, A. W. 2007, MNRAS, 380, 15

Ferguson, A. M. N., Irwin, M. J., Ibata, R. A., Lewis, G. F. and Tanvir, N. R. 2002, AJ, 124, 1452

Geehan, J. J., Fardal, M. A., Babul, A. and Guhathakurta, P. 2006, MNRAS, 366, 996

Gilbert, K. M., Guhathakurta, P., Kollipara, P., et al. 2009, ApJ, 705, 1275

Gilbert, K. M., Tollerud, E., Beaton, R. L., et al. 2018, ApJ, 852, 128

Guhathakurta, P., Rich, R. M., Reitzel, D. B., et al. 2006, AJ, 131, 2497

Hammer, F., Yang, Y. B., Wang, J. L., et al. 2018, MNRAS, 475, 2754

Hood, C. E., Kannappan, S. J., Stark, D. V., et al. 2018, ApJ, 857, 144

Ibata, R., Irwin, M., Lewis, G., Ferguson, A. M. N. and Tanvir, N. 2001, Natur, 412, 49

Ibata, R., Chapman, S., Ferguson, A. M. N., et al. 2004, MNRAS, 351, 117

Ibata, R., Martin, N. F., Irwin, M., et al. 2007, ApJ, 671, 1591

Johnston, K. V., Bullock, J. S., Sharma, S., et al. 2008, ApJ, 689, 936

Karademir, G. S., Remus, R.-S., Burkert, A., et al. 2019, MNRAS, 487, 318

Longobardi, A., Arnaboldi, M., Gerhard, O., Pulsoni, C. and Söldner-Rembold, I. 2018, A&A, 620, A111

Martínez-Delgado, D., Gabany, R. J., Crawford, K., et al. 2010, AJ, 140, 962

Mathewson, D. S., Cleary, M. N. and Murray, J. D. 1974, ApJ, 190, 291

McConnachie, A. W., Irwin, M. J., Ibata, R. A., et al. 2003, MNRAS, 343, 1335

Merritt, A., van Dokkum, P., Abraham, R. and Zhang, J. 2016, ApJ, 830, 62

Miki, Y., Mori, M. and Rich, R. M. 2016, ApJ, 827, 82

Milošević, S., Mićić, M. and Lewis, G. F. 2022, MNRAS, 511, 2868

Navarro, J. F., Frenk, C. S. and White, S. D. M. 1996, ApJ, 462, 563

Pillepich, A., Vogelsberger, M., Deason, A., et al. 2014, MNRAS, 444, 237

Purcell, C. W., Bullock, J. S. and Zentner, A. R. 2007, ApJ, 666, 20

Putman, M. E., de Heij, V., Staveley-Smith, L., et al. 2002, AJ, 123, 873

Remus, R.-S., Burkert, A. and Dolag, K. 2017, in Formation and Evolution of Galaxy Outskirts, ed. A. Gil de Paz, J. H. Knapen, and J. C. Lee, Vol. 321, 84–86

Sadoun, R., Mohayaee, R. and Colin, J. 2014, MNRAS, 442, 160

Springel, V. 2005, MNRAS, 364, 1105

Wannier, P. and Wrixon, G. T. 1972, ApJL, 173, L119

Widrow, L. M., Pym, B. and Dubinski, J. 2008, ApJ, 679, 1239

Zolotov, A., Willman, B., Brooks, A. M., et al. 2009, ApJ, 702, 1058

ЗАВИСНОСТ ЗВЕЗДАНИХ ПОДСТРУКТУРА У ГАЛАКСИЈАМА ТИПА М31 ОД МОРФОЛОГИЈЕ САТЕЛИТА У СУДАРИМА ГАЛАКСИЈА

S. Milošević

University of Belgrade, Department of Astronomy at Faculty of Mathematics,
Studentski trg 16, 11000 Belgrade, Serbia

E–mail: *stanislav@matf.bg.ac.rs*

Звездани токови и љуске су посматрани у халоима спиралних галаксија. У овом раду истражујемо формирање ових структура, насталих у сударима спиралне галаксије са патуљастом галаксијом која је њен сателит. Извршене су симулације N тела са два морфолошка типа патуљасте галаксије за различите почетне позиције. Један модел је сфероидна патуљаста галаксија, а други патуљаста галаксија са диском. Утврдили смо да оба модела могу да формирају токове и љуске и да су токови у случају патуљасте галаксије са диском више изражени. Након неколико орбита, у овом случају могуће је формирање и више токова. Остатак галаксије се касније распада у случају патуљасте галаксије са диском у односу на сфероидну.